

Optimal three-body correlations and elementary diagrams in liquid ⁴He

E. Krotscheck

*Department of Physics, Texas A&M University, College Station, Texas 77843
and Max-Planck-Institut für Kernphysik, D-6900 Heidelberg, West Germany**

(Received 13 May 1985; revised manuscript received 28 October 1985)

Within the framework of the variational theory for strongly interacting Bose liquids, we study the optimal determination of three-body correlation factors. The Euler-Lagrange equation for the three-body correlations suggests an iterative procedure in which the three-body correlation factor is expressed as a series of diagrams containing only the pair distribution function. The long-wavelength behavior of the three-body structure function agrees formally with the prediction of quantum hydrodynamics. The simplest approximation for the optimized three-body correlation function is identical to the prediction of second-order correlated-basis-function perturbation theory. We show that this simplest approximation sums essentially the same sets of diagrams that are included in non-optimized hypernetted-chain calculations with three-body correlations. Along with the three-body correlations we include those elementary diagrams of fourth and fifth order which have a comparable topological structure. The predictions for the ground-state energy and the pair distribution function are substantially improved compared with hypernetted-chain calculations restricted to two-body correlations.

I. INTRODUCTION

Much of the success in the present microscopic understanding of quantum liquids has been initiated by the observation that the exact ground state of a Bose system can be written in the form

$$\Psi_0(\mathbf{r}_1, \mathbf{r}_2, \dots, \mathbf{r}_A) = \exp \left[\frac{1}{2} \left[\sum_{i=1}^A u_1(\mathbf{r}_i) + \sum_{\substack{i,j=1 \\ i < j}}^A u_2(\mathbf{r}_i, \mathbf{r}_j) + \sum_{\substack{i,j,k=1 \\ i < j < k}}^A u_3(\mathbf{r}_i, \mathbf{r}_j, \mathbf{r}_k) + \dots \right] \right]. \quad (1.1)$$

The cause for the success of this idea¹ is that the form (1.1) of the wave function, the so-called Feenberg form,² allows in a relatively straightforward way the accurate calculation of expectation values, either by integral-equation methods¹ or by direct Monte Carlo integration.³ Integral equation methods such as the hypernetted chain (HNC) summations are less accurate than Monte Carlo integrations, but it is easier to assess fine details (such as the long-ranged behavior,¹ or anisotropies in an inhomogeneous system⁴) by the optimization of the correlation factors $u_n(\mathbf{r}_1, \mathbf{r}_2, \dots, \mathbf{r}_n)$ through solving the variational problems

$$\frac{\delta E}{\delta u_n(\mathbf{r}_1, \mathbf{r}_2, \dots, \mathbf{r}_n)} = 0 \quad (n = 1, 2, 3, \dots). \quad (1.2)$$

The optimization of the correlation functions is an important prerequisite for the study of the low-lying excited states of the system. Apart from this, the correlation factors obtained by optimization can also be used successful-

ly⁵ in more accurate Monte Carlo evaluations of the energy expectation value

$$E = \frac{\langle \Psi_0 | H | \Psi_0 \rangle}{\langle \Psi_0 | \Psi_0 \rangle}, \quad (1.3)$$

but it is much harder to use direct Monte Carlo methods as a guidance to find optimal pair correlations.⁶

Of course, it is not practical to solve Eq. (1.2) for all n , but it is fortunately sufficient to keep only the first few components of the wave function (1.1). The treatment of $n=1$ is necessary only in an inhomogeneous system.⁴ It leads to a generalized Hartree equation for the one-body density. We need not be concerned with that aspect of the theory in the present case of the bulk liquid.

An elegant and practical method for solving the Euler-Lagrange (1.2) for $n=2$ has been given by Campbell and Feenberg⁷ in their "paired phonon analysis" (PPA). The method has proven sufficiently efficient to be applied also in simple inhomogeneous systems.⁴ The wave function obtained by omitting all correlations for $n \neq 2$ is usually called the Jastrow choice.

The first serious approach to include three-body correlations in the wave function was reported somewhat later by Woo and Coldwell.⁸ Campbell and co-worker^{9,10} formulated a systematic optimization procedure for arbitrary n -body correlations in the form of a perturbation expansion. A superficial interpretation of these early studies seems to indicate that three-body effects are treated there in low order, and that the equivalent of HNC summations with three-body correlations¹¹ might be preferable. One of the results of this work show this to be incorrect, and the second-order correlated-basis-function (CBF) treatment of Campbell to be, when used with a re-optimization procedure for the two-body correlations, in fact of com-

parable diagrammatic structure to the work of Refs. 11.

A problem that is closely related to the structure of three-body correlations is the question of the so-called "elementary" diagrams. The hypernetted-chain approximation contains all the important formal ingredients of the ground-state correlations qualitatively correctly, but it fails to give the correct saturation energy and density. In order to achieve quantitative agreement of HNC type calculations with experiment or Monte Carlo simulations, these elementary diagrams must be included somehow. Some studies are found in the literature that calculate¹² the elementary diagrams or estimate their effect by "interpolation"¹³ or "scaling."¹⁴

From the viewpoint of a variational theory, the physical meaning of three-body correlations and elementary diagrams is different. While three-body correlations improve the wave function, elementary diagrams improve the accuracy of the energy evaluation for a given Jastrow wave function. From the viewpoint of perturbation theory, the two problems do not have a clear distinction. A careful analysis of the perturbation series for the ground-state energy^{15,16} shows that the Jastrow wave function fails at fourth order, while elementary diagrams contribute only sixth and higher-order corrections. This shows that one should first go beyond the Jastrow choice of the wave function before attempting to include elementary diagrams. One can easily see that essentially the same diagrammatic structures are involved in both the series of elementary diagrams and the three-body correlation effects. There is no point in including one effect while leaving the other one out.

A few words are in order here to justify the reconsideration of the problem of elementary diagrams and three-body correlations. The energy expectation value with respect to a Jastrow wave function is known from variational Monte Carlo calculations. A simpler, HNC-type calculation can at its best reproduce these results but yields in bulk ⁴He hardly any additional information. On the other hand, most of the important formal structure of the many-body problem (i.e., the ring and ladder diagrams) are contained in the HNC approximation, elementary diagrams contribute at most quantitative shifts of the general picture. Bridging the gap between the HNC approximation and variational Monte Carlo results is therefore, as a stand-alone task, a problem of a predominantly technical nature. The situation is a bit different for the three-body correlation function $u_3(\mathbf{r}_1, \mathbf{r}_2, \mathbf{r}_3)$. The study of the properties of this function gives insight into the structure of "backflow" correlations, which are hard to uncover from a wave function obtained by an exact Green's-function Monte Carlo (GFMC) solution of the Schrödinger equation. Conclusive information on the structure of the three-body correlations can be obtained of course only from an approach which determines three-

body correlation via the optimization procedure (1.2).

Among others, we have undertaken the present effort with the goal of applying the theory to inhomogeneous systems. In the surface or in thin films of liquid-⁴He systems, a wealth of experimental information is met by relatively little understanding of the correlations. The optimized Jastrow-HNC method provides a qualitatively reasonable⁴ description of the anisotropy of the correlations in these systems. But the predicted surface tension of liquid ⁴He is about a factor of 2 too small compared with the experiment, and improvements of the theory must be sought before reliable predictions can be made for the propagation of ripplons and third sound or on the behavior of impurities. We formulate, therefore, the theory with its extension to inhomogeneous systems in mind.

The paper is organized as follows: We give in the next section a brief discussion of the paired phonon analysis for the optimization of the two-body correlations. The energy expectation value in the presence of three-body correlations is calculated to sufficiently high order to allow for a meaningful unconstrained optimization. The derivation of the Euler-Lagrange equation for the three-body correlation factor is quite straightforward. We derive this equation only in the approximation in which we choose to work, but we display and discuss also the exact form of the equation. At the same time, the elementary diagrams are identified that give rise to the same topological structures as the three-body correlations.

Section III derives the long-wavelength behavior of the three-body static structure function as obtained by the inclusion of optimized three-body correlations. We show that one obtains a structural agreement with the prediction of quantum hydrodynamics.¹⁷ The last section, Sec. IV, describes our numerical procedure and presents the results. There, we have decided to treat elementary diagrams, as far as possible, in the old-fashioned way: we calculate them. Formulating the theory in momentum space leads to simplifications such that the relevant fifth-order elementary diagrams can be calculated from the four-body term without additional effort. Thus, we exhaust essentially the effect of the fourth- and fifth-order elementary diagrams calculated by Smith.¹² This brings the ground-state energy within 0.5 K of the GFMC results. This about as far as one can go without excessive numerical effort. To improve upon the accuracy, one may apply enhancement factors to the non-HNC contributions. Thus we adopt the idea, but not the ideology, of Ref. 14 on a much more modest scale.

II. ENERGY AND EULER-LAGRANGE EQUATIONS

Using the wave function (1.1) and including correlation factors up to $n=3$, we can write the energy expectation value of a translationally invariant system in the form

$$E = \frac{1}{2} \int d^3r_1 \int d^3r_2 \rho_2(|\mathbf{r}_1 - \mathbf{r}_2|) \left[v(|\mathbf{r}_1 - \mathbf{r}_2|) - \frac{\hbar^2}{4m} \nabla^2 u_2(|\mathbf{r}_1 - \mathbf{r}_2|) \right] - \frac{1}{3!} \frac{\hbar^2}{8m} \int d^3r_1 \int d^3r_2 \int d^3r_3 \rho_3(\mathbf{r}_1, \mathbf{r}_2, \mathbf{r}_3) (\nabla_1^2 + \nabla_2^2 + \nabla_3^2) u_3(\mathbf{r}_1, \mathbf{r}_2, \mathbf{r}_3). \quad (2.1)$$

In Eq. (2.1), $v(r)$ is the two-body interaction, and the $\rho_n(\mathbf{r}_1, \mathbf{r}_2, \dots, \mathbf{r}_n)$ are the familiar n -body densities. For further reference we introduce also the n -body distribution functions $g_n(\mathbf{r}_1, \mathbf{r}_2, \dots, \mathbf{r}_n) \equiv \rho_n(\mathbf{r}_1, \mathbf{r}_2, \dots, \mathbf{r}_n)/\rho^n$, where ρ is the one-body density. The two-body correlation factor $u_2(|\mathbf{r}_i - \mathbf{r}_j|)$ is renormalized to include, in a diagrammatic expansion, all those three-body terms that have one coordinate dependence integrated out, i.e., we define

$$\bar{u}_2(|\mathbf{r}_1 - \mathbf{r}_2|) \equiv u_2(|\mathbf{r}_1 - \mathbf{r}_2|) + \rho \int d^3r_3 u_3(\mathbf{r}_1, \mathbf{r}_2, \mathbf{r}_3). \quad (2.2)$$

Using (2.2), the energy expectation value (2.1) takes the form

$$E = E_{(2)} + E_{(3)} \quad (2.3)$$

with

$$E_{(2)} = \frac{\rho^2}{2!} \int d^3r_1 \int d^3r_2 g(\mathbf{r}_1, \mathbf{r}_2) \left[v(|\mathbf{r}_1 - \mathbf{r}_2|) - \frac{\hbar^2}{4m} \nabla^2 \bar{u}_2(|\mathbf{r}_1 - \mathbf{r}_2|) \right], \quad (2.4)$$

$$E_{(3)} = -\frac{\hbar^2}{8m} \frac{\rho^3}{3!} \int d^3r_1 \int d^3r_2 \int d^3r_3 [g_3(\mathbf{r}_1, \mathbf{r}_2, \mathbf{r}_3) - g(\mathbf{r}_1, \mathbf{r}_2) - g(\mathbf{r}_1, \mathbf{r}_3) - g(\mathbf{r}_2, \mathbf{r}_3) + 2] \\ \times (\nabla_1^2 + \nabla_2^2 + \nabla_3^2) u_3(\mathbf{r}_1, \mathbf{r}_2, \mathbf{r}_3). \quad (2.5)$$

The optimization condition for the two-body correlations can be formulated in various ways; we present here the formulation that allows for the most efficient numerical implementation. In that formulation, a particle-hole interaction is defined as

$$V_{\text{p-h}}(|\mathbf{r}_1 - \mathbf{r}_2|) \equiv \frac{\delta^2 E}{\delta \rho_1(\mathbf{r}_1) \delta \rho_1(\mathbf{r}_2)}. \quad (2.6)$$

[To apply the algorithm (2.6), one has to allow for an infinitesimally small nonuniform density component and keep the two- and three-body correlation functions fixed.] This particle-hole interaction defines through linear response theory a density-density response function, from which one obtains the static form factor $S(k) = 1 + \rho \int d^3r [g(r) - 1] \exp(i\mathbf{k} \cdot \mathbf{r})$ via frequency integration. The case of the homogeneous system is especially simple. One finds

$$S(k) = \left[1 + \frac{4m}{\hbar^2 k^2} \tilde{V}_{\text{p-h}}(k) \right]^{-1/2}, \quad (2.7)$$

where the dimensionless Fourier transform

$$\tilde{f}(k) \equiv \rho \int d^3r \exp(i\mathbf{k} \cdot \mathbf{r}) f(r)$$

is denoted by a tilde. Of course, the energy functional must be sufficiently accurate to allow for an unconstrained variation with respect to either the two-body correlations or the pair distribution function $g(\mathbf{r}_1, \mathbf{r}_2) \equiv g(|\mathbf{r}_1 - \mathbf{r}_2|)$. The HNC theory provides the necessary information on acceptable approximation schemes. In the presence of three-body correlations, the HNC equations are

$$g(r) = \exp[\bar{u}(r) + N(r) + E_3(r) + E(r)], \quad (2.8) \\ \tilde{N}(k) = \frac{[S(k) - 1]^2}{S(k)}.$$

Here,

$$E_3(|\mathbf{r}_1 - \mathbf{r}_2|) \equiv \rho \int d^3r_3 [g(\mathbf{r}_1, \mathbf{r}_3)g(\mathbf{r}_2, \mathbf{r}_3) - 1] \\ \times u_3(\mathbf{r}_1, \mathbf{r}_2, \mathbf{r}_3), \quad (2.9)$$

and $E(r)$ is the familiar sum of elementary diagrams, which may now also contain three-body correlation functions $u_e(\mathbf{r}_i, \mathbf{r}_j, \mathbf{r}_k)$. It is convenient to use the HNC relations (2.8) to eliminate $\bar{u}_2(r)$ from the energy expectation value (2.4) in favor of the pair distribution function $g(r)$. Thus we arrive, for the two-body part of the energy per particle, at

$$E/A = \frac{\rho}{2} \int d^3r g(r) \left[v(r) - \frac{\hbar^2}{4m} \nabla^2 [\ln g(r) - N(r) - E_3(r) - E(r)] \right] + E_{(3)} \\ \equiv E_{\text{HNC}} + \Delta E_3 + \Delta E_e, \quad (2.10)$$

where

$$E_{\text{HNC}} = \frac{\rho}{2} \int d^3r g(r) \left[v(r) - \frac{\hbar^2}{4m} \nabla^2 [\ln g(r) - N(r)] \right] \quad (2.11)$$

is the energy per particle in HNC approximation,

$$\Delta E_3 = \frac{\hbar^2 \rho}{8m} \int d^3r g(r) \nabla^2 E_3(r) + E_{(3)} \quad (2.12)$$

is the contribution arising from three-body correlations, and

$$\Delta E_e = \frac{\hbar^2 \rho}{8m} \int d^3r g(r) \nabla^2 E(r) \quad (2.13)$$

is the contribution from elementary diagrams. The advantage of the formulation (2.10)–(2.13) is that three-body correlations enter the theory only through the Jackson-Feenberg kinetic energy $E_{(3)}$, the three-body con-

tribution $E_3(r)$ [cf. Eq. (2.9)] in the HNC equations, and the elementary diagram structures. The total energy functional which appears as a correction term in the particle-hole interaction $V_{p-h}(r)$, includes these corrections. The derivation of the new Euler-Lagrange equation is straightforward. We obtain the general form

$$V_{p-h}(r) = g(r)[v(r) + \Delta v(r)] + \frac{\hbar^2}{m} |\nabla \sqrt{g(r)}|^2 + [g(r) - 1]w_I(r), \tag{2.14}$$

where

$$\Delta v(r) = \frac{1}{\rho} \frac{\delta(\Delta E_3 + \Delta E_e)}{\delta g(r)} \tag{2.15}$$

is the correction term due to three-body correlations and elementary diagrams, and

$$\bar{w}_I(k) = -\frac{\hbar^2 k^2}{4m} [2S(k) - 1][1 - S^{-1}(k)]^2. \tag{2.16}$$

The next task is to derive a Euler-Lagrange equation for the three-body correlation factor $u_3(\mathbf{r}_i, \mathbf{r}_j, \mathbf{r}_k)$. To this end, one has to include at least all terms in the elementary diagram sum that contain two three-body factors and all terms in the three-body distribution function that contain at least one three-body factor. For consistency, the topologically corresponding diagrams containing only two-body distribution functions should be retained. Figure 1

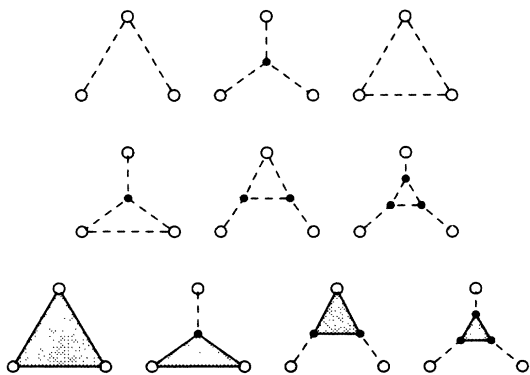


FIG. 1. Graphical representation of the connected part $g_3(\mathbf{r}_1, \mathbf{r}_2, \mathbf{r}_3) - g(\mathbf{r}_1, \mathbf{r}_2) - g(\mathbf{r}_1, \mathbf{r}_3) - g(\mathbf{r}_2, \mathbf{r}_3) + 2$ of the three-body distribution function. The representation is exact if the shaded triangle is interpreted as the set of all irreducible, non-nodal three-body diagrams. The set of diagrams included in the calculation of the three-body Jackson-Feenberg kinetic energy is the one obtained by approximating the shaded triangle by the three-body correlation function.

shows the diagrammatic representation of the terms that must be kept in the three-body factor

$$g_3(\mathbf{r}_1, \mathbf{r}_2, \mathbf{r}_3) - g(\mathbf{r}_1, \mathbf{r}_2) - g(\mathbf{r}_1, \mathbf{r}_3) - g(\mathbf{r}_2, \mathbf{r}_3) + 2.$$

We use the usual diagrammatic conventions: small circles represent the coordinates \mathbf{r}_i of particles, a dashed line between two points \mathbf{r}_i and \mathbf{r}_j represents a function $h(\mathbf{r}_i, \mathbf{r}_j) = g(\mathbf{r}_i, \mathbf{r}_j) - 1$, and a shaded triangle a three-body factor $u_3(\mathbf{r}_i, \mathbf{r}_j, \mathbf{r}_k)$. A solid dot implies integration over the coordinate space of the associated particle and a density factor. The representation of the three-body distribution function satisfies the sequential relation between $g_3(\mathbf{r}_1, \mathbf{r}_2, \mathbf{r}_3)$ and $g(\mathbf{r}_1, \mathbf{r}_2)$. Note that the graphical representation shown in Fig. 1 is *exact* if we interpret the shaded triangle as the sum of all three-point diagrams which are non-nodal in all three external points. (A diagram is called *nodal* in an external point if there exists an internal point through which all paths which connect that external point to any other external point must go.)

Figure 2 shows the sets of elementary diagrams that must be included. In particular, we see that the inclusion of these diagrams contains, after trivialization of the full three-body correlation factor, the so-called backflow form

$$u_3(\mathbf{r}_1, \mathbf{r}_2, \mathbf{r}_3) \approx [\nabla_1 \eta(|\mathbf{r}_1 - \mathbf{r}_2|) \cdot \nabla_1 \eta(|\mathbf{r}_1 - \mathbf{r}_3|) + \text{c.p.}],$$

where c.p. stands for cyclic permutations of 1,2,3. The approximation shown in Fig. 2 contains essentially all diagrams included in Refs. 11; it goes far beyond that work in the computation of the three-body kinetic energy (cf. Fig. 1).

After the relevant diagrammatic structures are identified, it is straightforward to derive a compact expression for the energy correction term. Since the calculation is somewhat tedious, we bypass the technical details. One works most conveniently in momentum space. We define

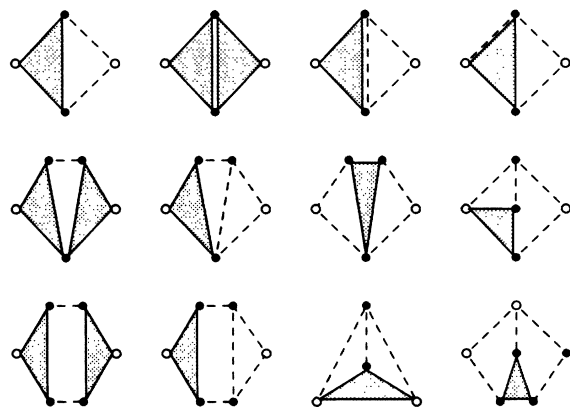


FIG. 2. Set of elementary diagrams included in the present calculation that contain one or two three-body correlation factors $u_3(\mathbf{r}_i, \mathbf{r}_j, \mathbf{r}_k)$.

$$\tilde{u}_3(\mathbf{k}_1, \mathbf{k}_2, \mathbf{k}_3) = \rho^2 \int d^3 r_{12} \int d^3 r_{13} \exp(i\mathbf{k}_1 \cdot \mathbf{r}_{12} + i\mathbf{k}_2 \cdot \mathbf{r}_{13}) u_3(\mathbf{r}_1, \mathbf{r}_2, \mathbf{r}_3), \quad (2.17)$$

with $\mathbf{r}_{ij} \equiv \mathbf{r}_i - \mathbf{r}_j$ and $\mathbf{k}_3 = -\mathbf{k}_1 - \mathbf{k}_2$. Additional abbreviations are

$$X_3(\mathbf{r}_1, \mathbf{r}_2, \mathbf{r}_3) \equiv h(r_{12})h(r_{13})h(r_{23}) \quad (2.18)$$

and

$$X'_3(\mathbf{r}_1, \mathbf{r}_2, \mathbf{r}_3) \equiv \left[\frac{\hbar^2}{4m} \right] [\nabla^2 h(r_{12})h(r_{13})h(r_{23}) + \text{c.p.}] \quad (2.19)$$

(The quantities X_3 and X'_3 have a more general definition, which will be given below.) In terms of these quantities and the set of "non-nodal" diagrams

$$X(r) \equiv g(r) - 1 - N(r),$$

the three-body contribution to the total energy is

$$\begin{aligned} \Delta E_3 = & \frac{1}{24(2\pi)^6 \rho^2} \frac{\hbar^2}{2m} \int d^3 k_1 \int d^3 k_2 \int d^3 k_3 \tilde{u}_3(\mathbf{k}_1, \mathbf{k}_2, \mathbf{k}_3) \\ & \times \left[[2\mathbf{k}_1 \cdot \mathbf{k}_2 \tilde{X}(k_1) \tilde{X}(k_2) + \text{c.p.}] + [k_1^2(1 - 2\tilde{X}(k_1) + \text{c.p.}) \tilde{X}_3(\mathbf{k}_1, \mathbf{k}_2, \mathbf{k}_3) \right. \\ & \left. + \frac{8m}{\hbar^2} \tilde{X}'_3(\mathbf{k}_1, \mathbf{k}_2, \mathbf{k}_3) \left[\frac{k_1^2}{S(k_1)} + \frac{k_2^2}{S(k_2)} + \frac{k_3^2}{S(k_3)} \right] \tilde{u}_3(\mathbf{k}_1, \mathbf{k}_2, \mathbf{k}_3) \right] \\ & \times S(k_1)S(k_2)S(k_3)\delta(\mathbf{k}_1 + \mathbf{k}_2 + \mathbf{k}_3). \quad (2.20) \end{aligned}$$

This form is easily minimized with respect to $u_3(\mathbf{k}_1, \mathbf{k}_2, \mathbf{k}_3)$, which leads to

$$\tilde{u}_3(\mathbf{k}_1, \mathbf{k}_2, \mathbf{k}_3) = -\delta_{\mathbf{k}_1 + \mathbf{k}_2 + \mathbf{k}_3, 0} \frac{[\mathbf{k}_1 \cdot \mathbf{k}_2 \tilde{X}(k_1) \tilde{X}(k_2) + \text{c.p.}] + \frac{1}{2} \{k_1^2 [1 - 2\tilde{X}(k_1)] + \text{c.p.}\} \tilde{X}_3(\mathbf{k}_1, \mathbf{k}_2, \mathbf{k}_3) + (4m/\hbar^2) \tilde{X}'_3(\mathbf{k}_1, \mathbf{k}_2, \mathbf{k}_3)}{k_1^2/S(k_1) + k_2^2/S(k_2) + k_3^2/S(k_3)}. \quad (2.21)$$

Equation (2.21) is more general in the sense that its algebraic structure is identical to the structure of the exact Euler-Lagrange equation for the three-body factor. The quantities $X_3(\mathbf{r}_1, \mathbf{r}_2, \mathbf{r}_3)$ and $X'_3(\mathbf{r}_1, \mathbf{r}_2, \mathbf{r}_3)$ must be defined more generally in that case: $X_3(\mathbf{r}_1, \mathbf{r}_2, \mathbf{r}_3)$ is the set of three-body diagrams in terms of the two-body correlations

$$f_2^2(r_{ij}) - 1 \equiv \exp[u_2(r_{ij})] - 1$$

and

$$f_3^2(\mathbf{r}_i, \mathbf{r}_j, \mathbf{r}_k) - 1 \equiv \exp[u_3(\mathbf{r}_i, \mathbf{r}_j, \mathbf{r}_k)] - 1$$

that is non-nodal in all three external points, *except* the three-body correlation factor $u_3(\mathbf{r}_1, \mathbf{r}_2, \mathbf{r}_3)$. The quantity $X'_3(\mathbf{r}_1, \mathbf{r}_2, \mathbf{r}_3)$ is obtained graphically from $X_3(\mathbf{r}_1, \mathbf{r}_2, \mathbf{r}_3)$ by replacing, in turn, all two-body bonds $f_2(r_{ij}) - 1$ by

$$f_2^2(r_{ij}) \left[v(r_{ij}) - \frac{\hbar^2}{4m} \nabla^2 u_2(|\mathbf{r}_i - \mathbf{r}_j|) \right],$$

and all three-body correlations $f_3^2(\mathbf{r}_i, \mathbf{r}_j, \mathbf{r}_k) - 1$ by

$$\frac{\hbar^2}{8m} f_3^2(\mathbf{r}_i, \mathbf{r}_j, \mathbf{r}_k) (\nabla_i^2 + \nabla_j^2 + \nabla_k^2) u_3(\mathbf{r}_i, \mathbf{r}_j, \mathbf{r}_k).$$

One can now also invoke the usual dressing procedure to

reduce $X_3(\mathbf{r}_1, \mathbf{r}_2, \mathbf{r}_3)$ and $X'_3(\mathbf{r}_1, \mathbf{r}_2, \mathbf{r}_3)$ to their "basic" structures by expressing them in terms of the pair distribution function $h(r) = g(r) - 1$ and (in X'_3) $\nabla^2 g(r)$ and $(\nabla_1^2 + \nabla_2^2 + \nabla_3^2)g_3(\mathbf{r}_1, \mathbf{r}_2, \mathbf{r}_3)$. The first contributions to the three-body quantities in this dressed representation is the superposition approximation given in Eqs. (2.18) and (2.19).

In Eq. (2.21) we recover the convolution approximation

$$\begin{aligned} \tilde{u}_3^{\text{CA}}(\mathbf{k}_1, \mathbf{k}_2, \mathbf{k}_3) = & -\delta_{\mathbf{k}_1 + \mathbf{k}_2 + \mathbf{k}_3, 0} \\ & \times \frac{\mathbf{k}_1 \cdot \mathbf{k}_2 \tilde{X}(k_1) \tilde{X}(k_2) + \text{c.p.}}{k_1^2/S(k_1) + k_2^2/S(k_2) + k_3^2/S(k_3)} \quad (2.22) \end{aligned}$$

used by Chang and Campbell¹⁰ if we neglect the non-nodal three-body quantities X_3 and X'_3 . The first correction term to the convolution approximation is the superposition approximation, (2.18) and (2.19), which can be written as

$$\begin{aligned} & (\nabla_1^2 + \nabla_2^2 + \nabla_3^2) X_3(\mathbf{r}_1, \mathbf{r}_2, \mathbf{r}_3) - \frac{8m}{\hbar^2} X'_3(\mathbf{r}_1, \mathbf{r}_2, \mathbf{r}_3) \\ & \approx 2[\nabla h(r_{12}) \cdot \nabla h(r_{13}) h(r_{23}) + \text{c.p.}] \quad (2.23) \end{aligned}$$

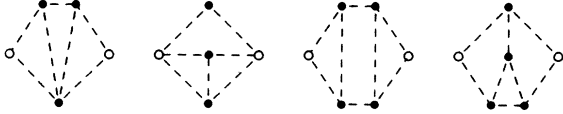


FIG. 3. Four-, five, and six-body elementary diagrams in terms of the pair distribution factor $g(r)-1$ that correspond to those shown in Fig. 2.

The generalized definition for X_3 and X'_3 provides a systematic route to improve upon the three-body correlations. But we will see that the correction term (2.23) is, in the vicinity of the saturation density, only a rather small modification of the convolution approximation (2.22). The convolution approximation (2.22) should therefore be adequate for most practical purposes. We see also that the so-called backflow form of Refs. 11 can be obtained by setting the energy denominator in the convolution approximation (2.22) equal to a constant. More conventionally, however, one means with backflow a current-current coupling term in the particle-hole interaction. The particle hole interaction (2.14) derived from any variational ground-state theory is local independently of the presence of three-body correlations. One hesitates therefore to identify correlations of the structure (2.22) with the Feynman-Cohen backflow. These correlations should more appropriately be identified with static three-body correlations; a relation to the Feynman-Cohen backflow cannot be derived from a ground-state theory.

The remaining task is the calculation of the elementary diagrams of a topological structure equivalent to the ones kept for the three-body correlations. These diagrams are shown in Fig. 3. For a given approximation for the three-body correlations and the choice of the elementary diagrams one may now also make a comparison with the perturbation series of the ground state of a weakly interacting Bose system. The relation between this perturbation series and the optimized Jastrow-HNC approximation has been studied most thoroughly by Jackson *et al.*¹⁶ who find that the Jastrow-HNC approximation fails in fourth order of the perturbation series. One can easily verify that the inclusion of three-body correlations in the

convolution approximation (2.25) is exact to at least fourth order in the energy. Higher-order terms in the perturbation series are not available in the literature. Since the superposition approximation for X_3 and X'_3 plus the set of elementary diagrams shown in Fig. 3 exhausts all diagrams up to fifth order in the pair correlation function, we conjecture that this approximation gives the energy of a weakly interacting Bose system correctly up to the fifth order.

III. THREE-BODY STATIC FORM FACTOR

The graphical representation of the connected part $g_3(\mathbf{r}_1, \mathbf{r}_2, \mathbf{r}_3) - g(\mathbf{r}_1, \mathbf{r}_2) - g(\mathbf{r}_1, \mathbf{r}_3) - g(\mathbf{r}_2, \mathbf{r}_3) + 2$ of the three-body distribution function shown in Fig. 1 leads, for the three-body static structure factor, to the exact representation

$$S(\mathbf{k}_1, \mathbf{k}_2, \mathbf{k}_3) = \delta_{\mathbf{k}_1 + \mathbf{k}_2 + \mathbf{k}_3, 0} S(k_1) S(k_2) S(k_3) \times [1 + \tilde{u}_3(\mathbf{k}_1, \mathbf{k}_2, \mathbf{k}_3) + \tilde{X}_3(\mathbf{k}_1, \mathbf{k}_2, \mathbf{k}_3)]. \quad (3.1)$$

The first term in Eq. (3.1) is the ordinary convolution approximation, the remaining terms are the corrections due to the inclusion of three-body correlations and Abe diagrams. To be able to make general statements about the three-body structure factor we must, of course, assume throughout this section that $X_3(\mathbf{r}_1, \mathbf{r}_2, \mathbf{r}_3)$ and $X'_3(\mathbf{r}_1, \mathbf{r}_2, \mathbf{r}_3)$ are included exactly in the sense of the diagrammatic definition given in the preceding section. $X_3(\mathbf{r}_1, \mathbf{r}_2, \mathbf{r}_3)$ and $X'_3(\mathbf{r}_1, \mathbf{r}_2, \mathbf{r}_3)$ are short-ranged functions, and the long-wavelength behavior of the two-body quantities $S(k)$ and $X(k)$ is

$$S(k) \sim \frac{\hbar k}{2mc_*} \text{ as } k \rightarrow 0+ \quad (3.2)$$

and

$$\tilde{X}(k) = 1 - 1/S(k) \sim -2mc_*/\hbar k \text{ as } k \rightarrow 0+, \quad (3.3)$$

where c_* is the velocity of sound predicted by the long-wavelength limit of the particle hole interaction (2.14),

$$mc_*^2 \equiv \tilde{V}_{p-h}(0+). \quad (3.4)$$

Keeping in Eq. (2.21) only the contributions that dominate as $k_i \rightarrow 0$ ($i=1,2,3$), we find

$$\tilde{u}(\mathbf{k}_1, \mathbf{k}_2, \mathbf{k}_3) = -\delta_{\mathbf{k}_1 + \mathbf{k}_2 + \mathbf{k}_3, 0} \frac{[\mathbf{k}_1 \cdot \mathbf{k}_2 \tilde{X}(k_1) \tilde{X}(k_2) + \text{c.p.}] + (4m/\hbar^2) \tilde{X}'_3(0,0,0)}{k_1^2/S(k_1) + k_2^2/S(k_2) + k_3^2/S(k_3)} \text{ as } k_i \rightarrow 0+. \quad (3.5)$$

The three-body correlation function \tilde{u}_3 dominates the long-wavelength behavior of the three-body structure function (3.1):

$$S(\mathbf{k}_1, \mathbf{k}_2, \mathbf{k}_3) = -\delta_{\mathbf{k}_1 + \mathbf{k}_2 + \mathbf{k}_3, 0} \left[\frac{\hbar}{2mc_*} \right]^2 \frac{k_1 k_2 k_3}{k_1 + k_2 + k_3} \times \left[\frac{\mathbf{k}_1 \cdot \mathbf{k}_2}{k_1 k_2} + \text{c.p.} + \frac{\tilde{X}'_3(0,0,0)}{mc_*^2} \right]. \quad (3.6)$$

The form (3.6) of the long-wavelength structure is identical to the one derived by Berdahl from a quantum-hydrodynamic model.¹⁷ There, the constant $\tilde{X}'_3(0,0,0)$ has been connected to the Grüneisen constant

$$u = \frac{\rho}{c} \frac{dc}{d\rho}. \quad (3.7)$$

To make a similar connection in our variational model, we follow the diagrammatic derivation of Ref. 18 for the connection between the quantity c_* [cf Eq. (3.4)] and the

hydrodynamic velocity of sound

$$mc^2 = \frac{d}{d\rho} \left[\rho^2 \frac{d(E/A)}{d\rho} \right]. \quad (3.8)$$

(Note that c and c_* are identical only for the *exact* ground-state wave function.)

A diagrammatic construction of the quantity $X'_3(\mathbf{r}_1, \mathbf{r}_2, \mathbf{r}_3)$ starts from the energy expectation value E/A . We assume E/A to be represented by a series of n -body diagrams; each of these diagrams carries a factor ρ^{n-1} ; thus, we write

$$E/A = \sum_{n=2}^{\infty} \rho^{n-1} e_n, \quad (3.9)$$

where the e_n depend on the density only through the density dependence of the optimal two- and three-body correlations. The set of non-nodal diagrams $X'_3(\mathbf{r}_1, \mathbf{r}_2, \mathbf{r}_3)$ can be obtained from such a graphical expansion of the energy by letting, in turn, each *triple* of internal points be external. Thus, each n -body diagram contributing to the ener-

gy generates $n(n-1)(n-2)$ diagrams contributing to $X'_3(\mathbf{r}_1, \mathbf{r}_2, \mathbf{r}_3)$. Taking the long-wavelength limit of this three-body function yields therefore an expansion in terms of the same diagrams as the energy, but with a weight factor $n(n-1)(n-2)$ for each n -body diagram, i.e.,

$$\tilde{X}'_3(0,0,0) = \sum_{n=3}^{\infty} n(n-1)(n-2) \rho^{(n-1)} e_n. \quad (3.10)$$

If we ignore the density dependence of the optimal correlation functions, we can also calculate the Grüneisen constant from the energy expansion (3.9) and obtain

$$u_* = \frac{1}{2mc_*^2} \sum_{n=2}^{\infty} n(n-1)^2 \rho^{n-1} e_n. \quad (3.11)$$

In other words, we arrive at the relation

$$\tilde{X}'_3(0,0,0) = mc_*^2 (2u_* - 1), \quad (3.12)$$

and obtain for the long-wavelength part of the three-body structure function

$$S(\mathbf{k}_1, \mathbf{k}_2, \mathbf{k}_3) = -\delta_{\mathbf{k}_1 + \mathbf{k}_2 + \mathbf{k}_3, 0} \left[\frac{\hbar}{2mc_*} \right]^2 \frac{k_1 k_2 k_3}{k_1 + k_2 + k_3} \left[\left(\frac{\mathbf{k}_1 \cdot \mathbf{k}_2}{k_1 k_2} + \text{c.p.} \right) + 2u_* - 1 \right] \text{ as } k_i \rightarrow 0. \quad (3.13)$$

We find, therefore, exactly the same situation as for the two-body structure function in the sense that the equivalence of the hydrodynamic prediction agrees with the prediction of the variational model only if the density dependence of the optimal correlation functions is negligible. The rigorous equivalence of the sound velocities c

and c_* has so far not been demonstrated in the variational model for any finite truncation of the Feenberg function (1.1).

It is also interesting to examine the long-wavelength behavior of the optimal three-body correlations. Using (3.3) in (3.5), we find

$$\tilde{u}_3(\mathbf{k}_1, \mathbf{k}_2, \mathbf{k}_3) = -\delta_{\mathbf{k}_1 + \mathbf{k}_2 + \mathbf{k}_3, 0} \left[\frac{2mc_*}{\hbar} \right] \frac{\{ (\mathbf{k}_1 \cdot \mathbf{k}_2 / k_1 k_2 + \text{c.p.}) + [\tilde{X}'_3(0,0,0) / mc_*^2] \}}{k_1 + k_2 + k_3} \text{ as } k_i \rightarrow 0. \quad (3.14)$$

The result (3.14) allows interesting conclusions on the density dependence of the three-body correlations in the vicinity of the spinodal point $c_* \rightarrow 0$: In this limit, the contribution from the convolution approximation vanishes, whereas the correction term becomes the dominant one.

We have given here, to our knowledge, the first microscopic derivation of the structure of the long-ranged portion of the three-body structure function. The derivation has been general enough such that one does not expect the result to be changed by the inclusion of four-body correlations. We have provided a proof that Berdahl's hydrodynamic model leads to the correct analytic form. The identification of our u_* with the exact Grüneisen constant is not yet completely clear, but we expect that the discrepancy is due to the finite truncation of the Feenberg function (1.1).

IV. NUMERICAL PROCEDURES AND RESULTS

In our numerical work we have adopted the superposition approximation (2.18) for the irreducible three-body

quantities contributing to the three-body correlations. It is very economical to evaluate the elementary diagrams in momentum space: In that case, the five- and six-body contributions to the energy arising from the elementary diagrams shown in Fig. 3 can be obtained without any extra effort from the ingredients of the four-body elementary diagram. We have not included in the numerical evaluation the six-body diagrams: these are only a small set of all six-body elementary diagrams and are repulsive, whereas the sum of all sixth-order elementary diagrams is attractive.¹² The question is immaterial for the corresponding triplet-correlation terms: their contribution to the energy is only of the order of 0.1 K at saturation density. We show in Table I the contribution to the ground-state energy from HNC diagrams E_{HNC} , triplet correlations in the convolution approximation of Campbell, $E_3^{(3)}$, and the four-, five-, and six-body corrections $E_3^{(4)}$. Also shown is the contribution to the energy from four- and five-body elementary diagrams, $E_e^{(4)}$ and $E_e^{(5)}$, respectively. These values agree reasonably well with the calculations of Smith.¹² We expect therefore that the two five-

TABLE I. Contributions to the ground-state energy (column 7) from two-body Jastrow correlations in the HNC-EL approximation E_{HNC} (column 2), the three-body part $\Delta E_3^{(3)}$ (column 3) and the four-body and higher-order terms $\Delta_3^{(4)}$ (column 4) arising from three-body correlations, and the contributions $\Delta E_e^{(4)}$ from fourth-order (column 5) and $\Delta E_e^{(5)}$ from fifth-order (column 6) elementary diagrams as a function of density ρ . Also shown is the velocity of sound c (column 8) as obtained from Eq. (3.8).

ρ (\AA^{-3})	E_{HNC} (K)	$\Delta E_3^{(3)}$ (K)	$\Delta E_3^{(4)}$ (K)	$\Delta E_e^{(4)}$ (K)	$\Delta E_e^{(5)}$ (K)	E (K)	c (m/sec)
0.016	-5.39	-0.34	0.03	-0.18	-0.28	-6.16	119
0.017	-5.42	-0.41	0.04	-0.21	-0.34	-6.35	151
0.018	-5.39	-0.50	0.05	-0.25	-0.40	-6.49	178
0.019	-5.28	-0.61	0.06	-0.30	-0.47	-6.59	202
0.020	-5.08	-0.73	0.07	-0.35	-0.55	-6.64	223
0.021	-4.79	-0.87	0.08	-0.41	-0.63	-6.62	240
0.022	-4.41	-1.04	0.09	-0.47	-0.72	-6.54	255
0.023	-3.92	-1.23	0.10	-0.55	-0.81	-6.40	266
0.024	-3.32	-1.44	0.12	-0.63	-0.91	-6.19	272

TABLE II. Same as Table I for the case where the pair distribution function is not reoptimized.

ρ (\AA^{-3})	E_{HNC} (K)	$\Delta E_3^{(3)}$ (K)	$\Delta E_3^{(4)}$ (K)	$\Delta E_e^{(4)}$ (K)	$\Delta E_e^{(5)}$ (K)	E (K)	c (m/sec)
0.016	-5.43	-0.29	0.03	-0.16	-0.26	-6.11	128
0.017	-5.48	-0.35	0.04	-0.19	-0.31	-6.29	161
0.018	-5.46	-0.42	0.05	-0.22	-0.36	-6.42	189
0.019	-5.36	-0.50	0.05	-0.26	-0.42	-6.50	215
0.020	-5.20	-0.60	0.06	-0.30	-0.49	-6.52	238
0.021	-4.94	-0.70	0.07	-0.34	-0.56	-6.47	258
0.022	-4.60	-0.82	0.08	-0.39	-0.63	-6.36	276
0.023	-4.15	-0.96	0.09	-0.45	-0.71	-6.17	291
0.024	-3.61	-1.11	0.11	-0.50	-0.79	-5.90	302

TABLE III. Same as Table I for the case where enhancement factors are applied to the three-body and elementary-diagram terms in order to fit the GFMC ground-state energy.

ρ (\AA^{-3})	E_{HNC} (K)	$\Delta E_3^{(3)}$ (K)	$\Delta E_3^{(4)}$ (K)	$\Delta E_e^{(4)}$ (K)	$\Delta E_e^{(5)}$ (K)	E (K)	c (m/sec)
0.017	-5.32	-0.53	0.05	-0.31	-0.49	-6.61	122
0.018	-5.26	-0.65	0.06	-0.37	-0.59	-6.81	151
0.019	-5.10	-0.80	0.07	-0.44	-0.69	-6.96	174
0.020	-4.86	-0.97	0.08	-0.52	-0.81	-7.07	195
0.021	-4.51	-1.17	0.10	-0.61	-0.93	-7.13	211
0.022	-4.05	-1.41	0.11	-0.72	-1.07	-7.13	225
0.023	-3.46	-1.69	0.13	-0.84	-1.21	-7.09	234
0.024	-2.75	-2.02	0.15	-0.99	-1.37	-6.98	238

body diagrams shown in Fig. 3 provide a reasonable approximation to the set of all elementary five-body diagrams.

The binding energy obtained here has a minimum of -6.64 K at a density of about 0.02 \AA^{-3} . The improvement over the Jastrow-HNC approximation is significant, but the energy still falls short of the GFMC value by about 0.5 K, we will return to this point further on.

The velocity of sound can be calculated from the equation of state through the hydrodynamic prediction (3.8) or, alternatively, from the long-wavelength limit of the spectrum of collective excitations, cf. Eq. (3.4). We have already mentioned that the two definitions will not necessarily lead to the same numerical value for the velocity of sound in any finite-order form of the Feenberg function. But the numerical values for the velocity of sound obtained by the two expressions agree within about 10%, whereas the discrepancy is much larger if no elementary diagrams and three-body correlations are included. The close agreement between the results of two different expressions for the velocity of sound lends further credibility to our calculational scheme.

We have pointed out above that our treatment of the three-body correlations is only equivalent to a direct HNC summation with triplet correlations if the pair-distribution is reoptimized. This has been done for the results shown in Table I. For comparison, we show in Table II the same energies as calculated with the $g(r)$ obtained from the optimization of the Jastrow-HNC energy expectation value E_{HNC} . We see that the reoptimization leads to very little additional binding, but it affects the velocity of sound notably. The effects are more significant in the radial distribution function and the static form factor, where the reoptimization produces an enhancement of the nearest-neighbor peak.

It has been known for some time¹² that there are still significant contributions from the elementary diagram sums from sixth- and seventh-order diagrams. Since it is rather tedious and time consuming to compute these diagrams, methods have been sought^{13,14} to estimate these higher-order effects. A possible route¹⁴ is to apply an enhancement factor to the elementary diagram sum and impose some consistency condition, such as the agreement of different forms of the kinetic energy, to determine this enhancement ("scaling") factor. Other possible consistency requirements would be sequential relations between $g(r_1, r_2)$ and $g_3(r_1, r_2, r_3)$, or Born-Green-Yvon relations between the two- and three-body correlation factors and distribution functions. It is clear that any approximate theory will lead to various inconsistencies somewhere, and each consistency requirement will lead to different scaling factors. It seems hard to find rationalizations that are ultimately justifiable on a microscopic basis. We prefer therefore to determine the enhancement factor from what we want it to do. This is to produce agreement of the approximate calculation with GFMC data such that we can then apply the theory to problems not yet treated by GFMC methods, or even out of their reach. To produce this agreement, we need to enhance the elementary-diagram correction (ΔE_e) by a factor of 1.35 and the three-body correlation term by a factor of 1.18. The same

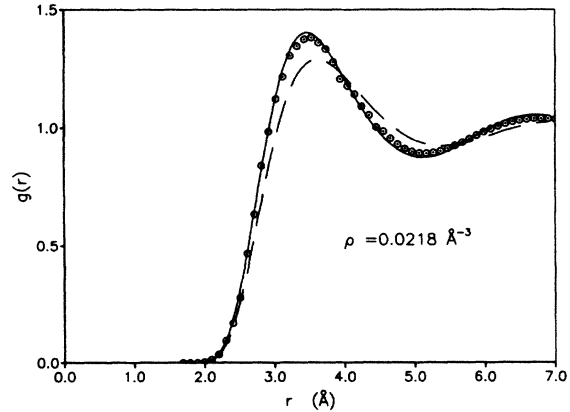


FIG. 4. Pair distribution function $g(r)$ from our calculation with enhancement factors (solid line) is compared with the GFMC data of Ref. 3 (circles) at the experimental saturation density $\rho = 0.02185 \text{ \AA}^{-3}$. The dashed line shows the optimized HNC approximation at the same density.

effect of enhancing the contribution from three-body correlations can be obtained by either omitting the terms $X_3(r_1, r_2, r_3)$ and $X'_3(r_1, r_2, r_3)$, or by replacing the Feynman spectrum in the energy denominator of Eq. (2.21) by bare kinetic energies. Two independent factors come in since we can compare independently $E_{\text{HNC}} + \Delta E_e$ with variational Monte Carlo calculations using the PPA pair correlation functions.⁶ Applying these factors, and keeping them constant over the whole density regime, gives the results of Table III, which show also that we obtain with that procedure a very reasonable estimate for the velocity of sound.

Figure 4 shows finally a comparison of our pair distribution function with the GFMC data from Ref. 3 for the calculation using enhancement factors. The comparison is satisfactory, but we note that the agreement between the pair distribution functions without the enhancement factor is even better. Since most of the structure of the nearest-neighbor peak is due to the three-body correlations, it seems that no enhancement factor should be applied there, and that some of the missing energy is in fact due to four-body effects.

To conclude, we emphasize that the main advantage of our procedure as compared with parametrized forms of two- and three-body correlations is that it requires no assumption whatsoever on specific analytic forms of these correlations. The optimization of the pair correlation function is hardly more complicated than the solution of the HNC equations with a given pair correlation function; it requires three instead of two Fourier transforms per iteration. The accuracy obtained as determined solely by the sets of "elementary" diagrams which one decides to include, and these determine the computational effort. The optimized approach provides, therefore, the *best possible* set of correlations, and does not increase the computational complexity. An interesting problem for further investigation is the connection to the parquet-diagram theory¹⁶ which produces a somewhat better agreement with GFMC results, if the ingredients of that theory corresponding to the variational elementary diagrams and three-body correlations are retained.¹⁹

ACKNOWLEDGMENT

I would like to thank C. E. Campbell for very useful remarks and suggestions.

*Present address.

¹E. Feenberg, *Theory of Quantum Liquids* (Academic, New York, 1969).

²J. W. Clark, Nucl. Phys. **328A**, 587 (1979).

³W. L. McMillan, Phys. Rev. **138**, A442 (1965).

⁴E. Krotscheck, G.-X. Qian, and W. Kohn, Phys. Rev. B **31**, 4245 (1985).

⁵M. H. Kalos, M. A. Lee, P. A. Whitlock, and G. Chester, Phys. Rev. B **24**, 115 (1981).

⁶F. J. Pinski and C. E. Campbell, Phys. Lett. **79B**, 23 (1978).

⁷C. E. Campbell and E. Feenberg, Phys. Rev. **188**, 396 (1969).

⁸C.-W. Woo and R. L. Coldwell, Phys. Rev. Lett. **29**, 1062 (1976).

⁹C. E. Campbell, Phys. Lett. **44A**, 471 (1973).

¹⁰C. C. Chang and C. E. Campbell, Phys. Rev. B **15**, 4238 (1977).

¹¹V. R. Pandharipande, Phys. Rev. B **18**, 218 (1978); K. E.

Schmidt and V. R. Pandharipande, *ibid.* **19**, 2504 (1979).

¹²R. A. Smith, Phys. Lett. **63B**, 369 (1976); **85B**, 183 (1976); R. A. Smith, A. Kallio, M. Puoskari, and P. Toropainen, Nucl. Phys. **328A**, 186 (1979).

¹³A. Fabrocini and S. Rosati, Nuovo Cimento **1D**, 567 (1982); **1D**, 615 (1982).

¹⁴Q. N. Usmani, B. Friedman and V. R. Pandharipande, Phys. Rev. B **25**, 4502 (1982); Q. N. Usmani, S. Fantoni, and V. R. Pandharipande, *ibid.* **26**, 6123 (1983).

¹⁵H. K. Sim, C.-W. Woo, and J. R. Buchler, Phys. Rev. A **2**, 2024 (1970).

¹⁶A. D. Jackson, A. Lande, and R. A. Smith, Phys. Rep. **86**, 55 (1982).

¹⁷P. Berdahl, Phys. Rev. A **10**, 2378 (1974).

¹⁸E. Krotscheck, Phys. Rev. A **15**, 397 (1977).

¹⁹A. D. Jackson, A. Lande, R. W. Guitink, and R. A. Smith, Phys. Rev. B **31**, 403 (1985).

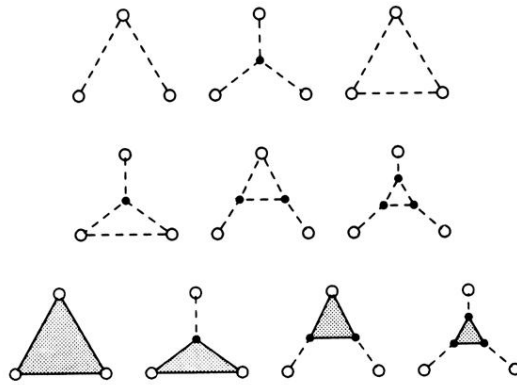


FIG. 1. Graphical representation of the connected part $g_3(\mathbf{r}_1, \mathbf{r}_2, \mathbf{r}_3) - g(\mathbf{r}_1, \mathbf{r}_2) - g(\mathbf{r}_1, \mathbf{r}_3) - g(\mathbf{r}_2, \mathbf{r}_3) + 2$ of the three-body distribution function. The representation is exact if the shaded triangle is interpreted as the set of all irreducible, non-nodal three-body diagrams. The set of diagrams included in the calculation of the three-body Jackson-Feenberg kinetic energy is the one obtained by approximating the shaded triangle by the three-body correlation function.

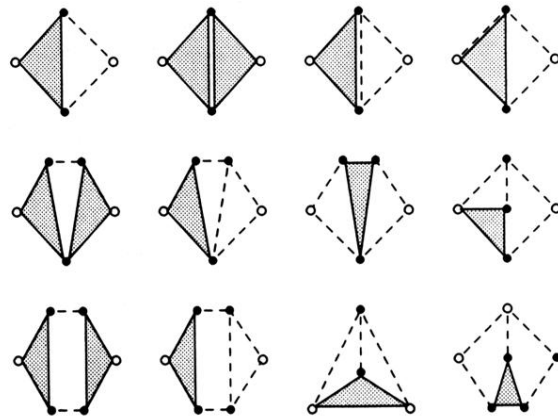


FIG. 2. Set of elementary diagrams included in the present calculation that contain one or two three-body correlation factors $u_3(\mathbf{r}_i, \mathbf{r}_j, \mathbf{r}_k)$.